Grid impedance estimation based hybrid islanding detection method for AC microgrids

Ghzaiel, Walid ; Jebali-Ben Ghorbal, Manel; Slama-Belkhodja, Ilhem ; Guerrero, Josep M.

Published in:
Mathematics and Computers in Simulation

DOI (link to publication from Publisher):
10.1016/j.matcom.2015.10.007

Publication date:
2017

Document Version
Early version, also known as pre-print

Accepted Manuscript

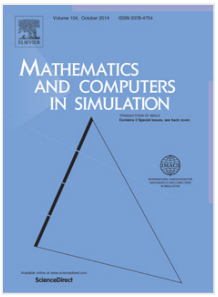

Grid impedance estimation based hybrid islanding detection method for AC microgrids

Walid Ghzaiel, Manel Jebali Ben Ghorbal, Ilhem Slama Belkhodja, Josep M. Guerrero

PII: S0378-4754(15)00221-9
DOI: http://dx.doi.org/10.1016/j.matcom.2015.10.007
Reference: MATCOM 4253

To appear in: *Mathematics and Computers in Simulation*

Received date: 22 October 2014
Revised date: 8 August 2015
Accepted date: 16 October 2015

Please cite this article as: W. Ghzaiel, M. Jebali Ben Ghorbal, I. Slama Belkhodja, J.M. Guerrero, Grid impedance estimation based hybrid islanding detection method for AC microgrids, Math. Comput. Simulation (2015), http://dx.doi.org/10.1016/j.matcom.2015.10.007

ELSEVIER

SciVerse ScienceDirect

Grid impedance estimation based hybrid islanding detection method for AC microgrids

Walid Ghzaiel[a], Manel Jebali Ben Ghorbal[a], Ilhem Slama Belkhodja[a] and Josep M. Guerrero[b]

[a]*Université de Tunis El Manar, ENIT, L.S.E.-, LR 11 ES 15, BP 37-1002, Tunis le Belvédère, Tunisie*
[b]*Aalborg University, Dept. Energy Technology, 9220 Aalborg, Denmark*

Abstract

This paper focuses on a hybrid islanding detection algorithm for parallel-inverters-based microgrids. The proposed algorithm is implemented on the unit ensuring the control of the intelligent bypass switch connecting or disconnecting the microgrid from the utility. This method employs a grid impedance estimation technique that uses resonance excitation once grid fault occurs. It includes two stages: the first one is to detect grid impedance variations resulting from a grid fault; and the second one is to excite the resonance by using a virtual resistance in order to extract the grid impedance parameters. Grid impedance variations detection algorithm is based on grid current measurements temporal redundancies with fast current acquisition period. Once the grid impedance variation is detected, the excitation resonance is performed by injecting a resonance frequency in only one inverter control to avoid interactions with other units. The selected inverter will be the one closest to the controllable distributed generation system or to a healthy grid side in case of meshed microgrid with multiple-grid connections. The detection algorithm is applied to quickly detect the resonance phenomena, so that the resonance excitation is canceled and the resistive and inductive grid impedance parts are estimated. Simulation results are carried out to illustrate the effectiveness of the proposed method.

Keywords: microgrid, islanding, grid impedance variation, resonance excitation, droop control method, virtual resistance.

1. Introduction

Microgrids (MGs) are emerging as a way to improve both power quality of the electrical grids by making them smarter and more flexible in the future. MGs should be able to operate connected to the utility grid or in island under grid fault conditions [16]. The transition between grid-connected and islanded modes relies on the islanding detection algorithm. The islanding operation depends on the electrical power quality at the point of common coupling (PCC) and the grid existence. Hence, two islanding scenarios can be considered:
- *Intentional or pre-planned islanding*: Symmetrical or unsymmetrical faults taking place somewhere in the grid will lead to voltage dips, frequency variations or unbalance problems that can be non-detected by the protection devices. In this case, local islanded detection algorithms are needed to disconnect the MG.
- *Non-intentional or unplanned islanding*: In this case, MG continues to supply local loads, while the main grid is disconnected from the PCC [18].
A non-detected islanding condition may lead to dangerous situation for utility personnel and cause damage to the distributed generation systems composing the MG. Hence, a reliable islanding detection method should be set in order to detect any islanding scenario at least as fast as required by standards. German standard (VDE-0126), for example, requires disconnection from the utility grid under grid impedance variation of 1Ω within 5s [12]. The detection should be available even under the worst conditions defined as a Non-Detection Zone (**NDZ**), in which MG active and reactive produced powers are completely consumed by the loads. In fact, pre-

planned islanding could be easily detected by respecting some stringent pre-defined standard. However, unplanned islanding, that is to say the failure of the grid, is more complicated to be detected since the voltage and frequency at PCC can be sustained in NDZ limits.

In the literature, several methods have been proposed for islanding detection due to the importance of this issue and its impact on the interconnected system behavior [19, 1, 14, 3, 8, 6]. These methods are mainly divided into two main categories: communication-based methods between the protection devices and the power generation system, and local methods that use only local measurements. Local methods can be classified into three subcategories: passive methods challenged by a large NDZ and an accurate suitable threshold; active methods that suffer from power quality degradation; and hybrid methods that tend to summarize the benefits of both passive and active methods. In this sense, a novel hybrid islanding detection method based on grid current measurements and resonance excitation is proposed in this paper. Indeed, at first, a passive method based on continuous grid current measurements allows the detection of any abrupt grid current variation at the PCC. Afterward, this passive method is combined with an active method based on the injection of the proper resonance frequency. Resonance excitation is carried out by implementing and varying a virtual resistance. This resistance helps, in grid connected mode, to improve the output power quality in healthy grid mode and to drive the system near the resonance once an abrupt grid current variation is detected. It also allows the discrimination of the variation causes: grid impedance variations [3] or load variation. This method is able to detect islanding conditions under any faulty condition even under the NDZ, the worst case, where other methods failed [8].

However, in a MG that comprises parallel inverters connected to the grid, the method application is more difficult due to the different proper resonance frequencies resulting from the impedance of each generation system. As consequence, resonance excitation of each inverter can damage the system and reduce the reliability of the MG**.** To overcome this problem, a MG control structure is proposed which derived from the structure of the parallel-inverters connected to double grid: the grid fault occurrence detection algorithm allows stiff grid determination and faulty grid one. Afterwards, in resonance excitation phase, only the closest distributed generation systems (DGSs) to the healthy grid remain connected to this utility grid while the others are disconnected. However, they are kept interconnected with controllable DGSs, such as gas engine, diesel generator or distributed storage system. These controllable DGSs can support voltage and frequency in islanded mode. The developed grid impedance parameters determination algorithm will be executed by the healthy grid closest DGS control.

This paper is organized as follows. The double grid-connected MG structure and the proposed MG control structure are reported in section II. The hybrid islanding method is introduced and discussed in section III with the different algorithm steps. Section IV is devoted to simulation results.

2. Microgrid architecture and control strategy

MGs generally include parallel distributed generation systems modeled by three-phases inverters connected to the utility grid through an LCL-filter for the non-controllable DGSs and LC-filter for the controllable DGSs. For simplicity, LCL-filters are used for both types of DGSs in this paper. The grid side filter inductance is considered as a line inductance, which increases the inductive character of output system impedance and helps for a proper parallel operation of controllable DGSs since they operate as voltage sources.

2.1. Microgrid with two grid connection points

For a meshed MG, the MG can be connected to a double grid through two intelligent bypass switches (**IBS**) in order to ensure better service continuity under grid faults. Fig. 1 presents a double grid-connected MG structure: parallel-inverters and loads remain grid-connected when grid-conditions guarantee a proper operation. In case of grid fault occurrence detected on one side of the double grid, the switches K_i, $i = 1,...4$ will close and open according to the grid failure in order to ensure healthy working of loads and DGSs and safety transfer of the electrical energy.

The proposed islanding method is based on a resonance injection for a specific period. This will have a negative impact due to the interaction between the parallel-inverters under resonance state. This interaction is a consequence of the line impedance between each inverter and the AC common bus. As a solution, an inverter with loads can remain connected to the healthy grid, whereas the other DGS excites the resonance to determine the grid impedance of the faulty grid. Hence, the estimated impedance values helps keeping the switch states decision.

2.2. Proposed microgrid structure

A controllable DGS (DG3), such as gas engine, diesel generator and distributed storage system, is included. It is connected to parallel inverters and behaves like a grid tracker in order to support the voltage and frequency in islanded mode. The non-controllable DGSs are inverters based on renewable power sources such as wind turbine (WTS) and photovoltaic systems (PVS). They act as current sources in grid connection mode. The system composed of controllable DGS, non-controllable DGS (DG2) and loads, is connected to the closest DGS from the grid (DG1) through a switch device noted K_1 and all the system is connected to the grid through an IBS, as depicted in Fig. 2. Indeed, grid impedance variations challenge the AC bus interfacing inverter control. In this way, the switch K_1 should be opened once a grid impedance variation was detected to avoid resonance problems in the MG caused by the interaction with the grid. Hence, controllable DG will, together with the parallel inverter DG2, supply the loads while the closest DG will execute the algorithm of grid impedance parameters determination to detect the islanding condition. As a consequence, different possible scenarios can occur as illustrated in Table 1.

Table 1. Proposed MG scenarios

IBS	K1	Scenario
ON	ON	Connected MG
ON	OFF	Connected DG
ON	Re-ON	Reconnected MG
Off	OFF	Islanded MG

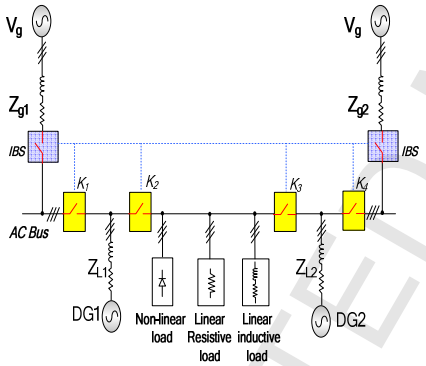

Fig. 1. Configuration of a MG connected to a double-grid

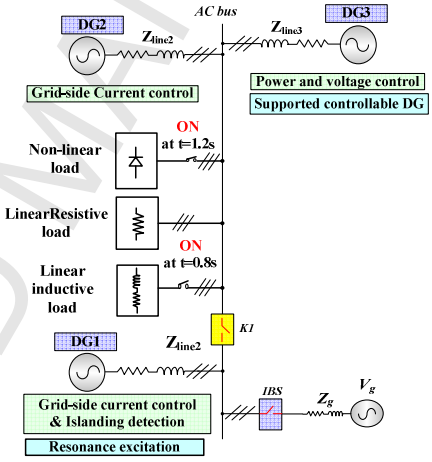

Fig. 2. Proposed MG structure control strategy

3. Proposed microgrid control strategy

In grid-connected mode, parallel non-controllable DGSs, such as PVS and WTS, behave like current sources (CS). Their control requires maximum power point tracking (MPPT) algorithm in order to sufficiently supply the loads and to inject the maximum power to grid. In this grid-connected mode, both frequency and voltage are supported by the grid. The controllable DGS acts as a voltage tracker, behaving like a voltage source, where its references are the grid voltage and frequency [8]. In islanded mode and during the execution of the algorithm explained hereinafter, the controllable DGS will change its references to support by itself the voltage and frequency while the parallel non-controllable DGSs are still working as current sources. Indeed, MG is usually designed so as to respect the following relations in order to avoid transmission power losses as follows

$$P_{MG} \geq \sum P_{Loads} \text{ and } Q_{MG} \geq \sum Q_{Loads} \quad (1)$$

However, in islanded mode, and with non-controllable DGSs based on MPPT, the produced MG power should not exceed the total demanded loads power. In this way, the installed non-controllable DGSs should have a maximum power less than the minimum total loads power as follows

$$P_{Loads\_\min} \leq \sum P_{DGs\_\max} \quad (2)$$

$$Q_{Loads\_\min} \leq \sum Q_{DGs\_\max} \quad (3)$$

The supported controllable DG acts hence as a grid source and a power balancer.

3.1. Non-controllable DGS strategy

As the non-controllable DGS behaves like a current source, its control strategy is based on controlling the grid side current. The voltage and frequency are imposed by the grid in grid-connected mode and supported by the controllable DGS in islanded mode. The continuous DC voltage is considered as constant by a prime source side converter and the grid model is an inductive resistive branch in series with an ideal voltage source noted V_g [18, 11].

Noteworthy that the high order LCL-filter can provoke the system instability which needs the integration of a damping element. For this reason, active damping is adopted as a solution and it is carried out by implementing a virtual resistance in the control strategy. In fact, it is done by multiplying the sensed filter-capacitor current by a predetermined gain noted R_v [3], and the result of this multiplication is subtracted from the converter voltage reference as depicted in Fig. 3. In the proposed microgrid structure, DG1; in which the proposed islanding detection algorithm is implemented and DG2 have the same current control strategy.

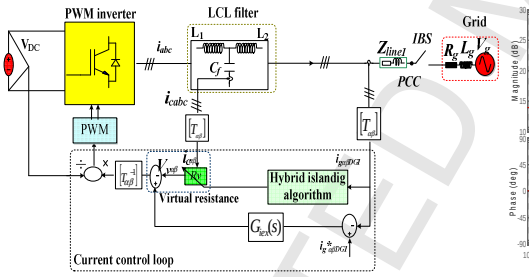

Fig. 3. Non-controllable DGS control strategy

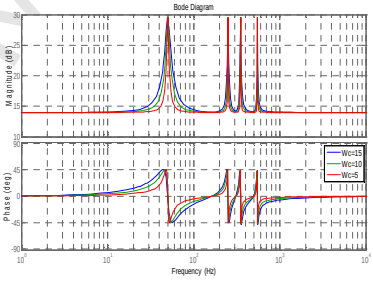

Fig. 4. Bode plot of multi-frequencies non-ideal P+R

For reliability and power quality reasons, a multi-frequencies non-ideal Proportional+Resonant (P+R) controller is used to control the output current in both DG1 and DG2. Its good regulation capability and its

harmonics suppression effect are proven in [13]. In the non-controllable DGS responsible for resonance excitation DG1, the transfer functions of the adopted (P+R) controller is given by:

$$G_{i_{ex}}(s)=k_{pex}+\frac{k_{rex}\,\omega_c\,s}{s^2+2\omega_c\,s+\omega^2}+\sum_{h=5,7,11}\frac{k_{rexh}\,\omega_c\,s}{s^2+2\omega_c\,s+\omega_h^2} \quad (4)$$

where k_{pex} is the proportional gain responsible for the system dynamic while k_{rex} is the resonant gain responsible for reducing the steady-state error. ω, ω_h, and ω_c are respectively the fundamental frequency, the harmonics frequencies and the cut-off frequency used for frequency fluctuation reducing as depicted in Fig. 4.

For more simplifications, grid-side current and reference voltage are expressed in the stationary reference as depicted in Fig. 3 using the Concordia transformation:

$$V_{\alpha\beta}=[T_{\alpha\beta}]V_{abc} \quad \text{and} \quad i_{\alpha\beta}=[T_{\alpha\beta}]i_{abc} \qquad [T_{\alpha\beta}]=\sqrt{\frac{2}{3}}\begin{bmatrix}1 & -\frac{1}{2} & -\frac{1}{2}\\ 0 & \frac{\sqrt{3}}{2} & -\frac{\sqrt{3}}{2}\end{bmatrix} \qquad [T_{\alpha\beta}^{-1}]=\sqrt{\frac{2}{3}}\begin{bmatrix}1 & 0\\ -\frac{1}{2} & \frac{\sqrt{3}}{2}\\ -\frac{1}{2} & -\frac{\sqrt{3}}{2}\end{bmatrix}$$

3.2. Controllable DGS control strategy

In grid-connected controllable DGS; considered as a voltage source, the active and reactive powers noted (*P* and *Q*) flowing from the filter output to the PCC through an inductor can be expressed as follows [17, 15]:

$$P=(\frac{EV}{Z}\cos\phi-\frac{V^2}{Z})\cos\theta+\frac{EV}{Z}\sin\phi\sin\theta \quad (5)$$

$$Q=(\frac{EV}{Z}\cos\phi-\frac{V^2}{Z})\sin\theta-\frac{EV}{Z}\sin\phi\cos\theta \quad (6)$$

ϕ is the angle phase between the controllable DG1 filter output and the PCC, *Z* is the inductor impedance, *E* is the DGS capacitor voltage amplitude, *V* is the PCC voltage amplitude and θ is the inductor impedance angle.

In this paper, droop method is used to control the controllable DGS and its principle is based on the two following assumptions:

1) The inductor impedance is purely inductive (Z=X, θ=90°). This assumption is true due to the large filtre inductance and power line impedance. But the resistive character of the power lines impedance in low voltage case can be a challenge. As a solution, virtual impedance can be added to the system control loops or using LCL-filter instead of LC one.
2) The angle ϕ is very small and assumed to be null ($\phi=0$, $\cos\phi=1$).

Based on these two assumptions, Eq. (5) and Eq. (6) can be expressed as shown below, where the DGS frequency is used instead of its angle phase

$$\omega=\omega^*-m(P-P^*) \quad (7)$$

$$E=E^*-n(Q-Q^*) \quad (8)$$

From Eq. (5) and Eq. (6), the relations *P/f* and *Q/E* can be deduced. In fact, an increase in the active and reactive powers leads to a decrease in the frequency and the voltage level respectively as can be shown in Fig. 5. Hence, the frequency and voltage can be considered as information about demanded power loads variation shared between the parallel inverters in real time.

However, the conventional droop method has the challenge of a slow transient response. In this sense, several

modified droop methods have been proposed in literature [4, 7, 5]. In this paper, derivative and integrator terms are added in droop equations to improve the system transient response. Hence, the equations will be expressed as:

$$\omega = \omega^* - m(P - P^*) - m_d \frac{d(P - P^*)}{dt} \quad (9) \quad \rightarrow \quad \phi = \phi^* - G_p(s)(P - P^*) \quad (11)$$

$$E = E^* - n(Q - Q^*) - n_d \int (Q - Q^*) \quad (10) \quad \rightarrow \quad E = E^* - G_q(s)(Q - Q^*) \quad (12)$$

ϕ is the phase of the V_c^*, $\phi^* = \omega^* \int dt = \omega^* t$,

$$G_p(s) = \frac{m_d\, s + m}{s} \quad (13)$$

$$G_q(s) = \frac{n_d\, s + n}{s} \quad (14)$$

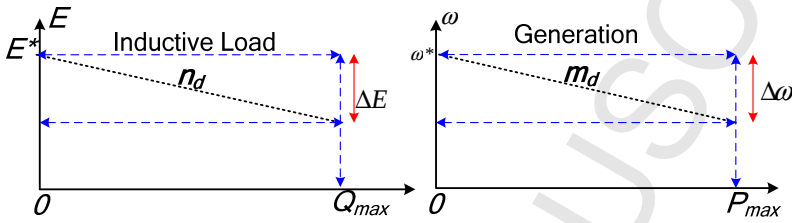

Fig. 5. Voltage and frequency droop principle

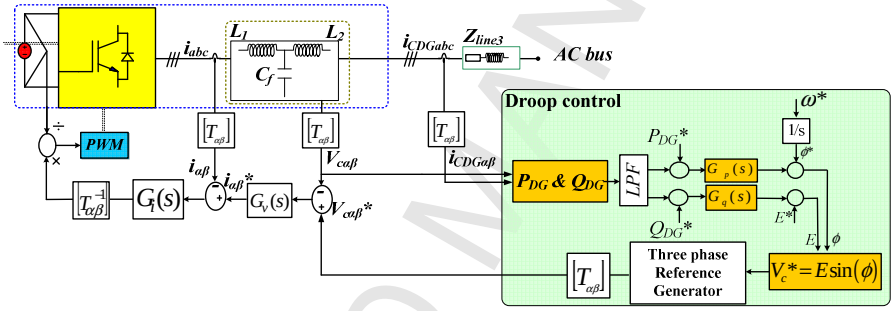

Fig.6. Controllable DGS control strategy

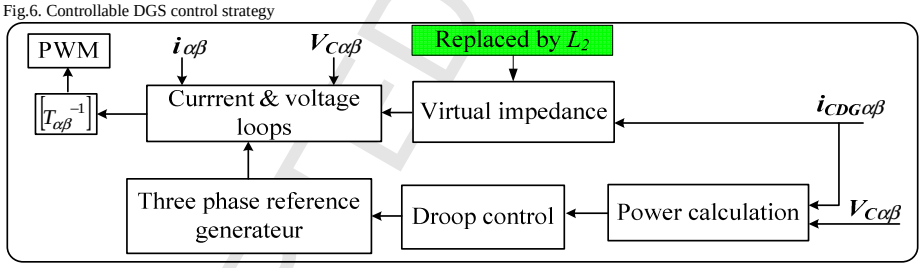

Fig. 7. Control structure based on 'Droop' control

Droop control inputs, active and reactive powers, are calculated from the unfiltered *p* and *q* power rich in ripple using first order low-pass-filter (LPF) as expressed in Eq. (15) and Eq. (16).

$$p = V_{c\alpha}\ i_{\alpha} + V_{c\beta}\ i_{\beta} \ \rightarrow\ P = \frac{\omega_c}{s+\omega_c}\, p \tag{15}$$

$$q = V_{c\beta}\ i_{\alpha} - V_{c\alpha}\ i_{\beta} \ \rightarrow\ Q = \frac{\omega_c}{s+\omega_c}\, q \tag{16}$$

The three voltage reference is deduced from the estimated voltage amplitude E^* and frequency ϕ as shown in Fig. 6 and it can be given by:

$$Vc^* = E\sin(\omega t) \tag{17}$$

The filter capacitor voltage and inverter current are both regulated by multi-frequencies non-ideal P+R controller where its transfer function is presented by:

$$G_v(s) = k_{pv} + \frac{k_{rv}\ \omega_c\ s}{s^2 + 2\omega_c\ s + \omega^2} + \sum_{h=5,7,11} \frac{k_{rvh}\ \omega_c\ s}{s^2 + 2\omega_c\ s + \omega_h^2} \tag{18}$$

$$G_i(s) = k_{pi} + \frac{k_{ri}\ \omega_c\ s}{s^2 + 2\omega_c\ s + \omega^2} + \sum_{h=5,7,11} \frac{k_{rih}\ \omega_c\ s}{s^2 + 2\omega_c\ s + \omega_h^2} \tag{19}$$

3.3. Synchronization

Many grid synchronization algorithms exist in the literature and their importance is growing due to its advanced role in performing an accurate synchronization and avoiding overcurrent. One of these synchronization algorithms is the second order generalized integrator SOGI that is adopted in this paper since it is characterized by its high efficiency under unbalance or perturbation as proven in literature [12] and [13]. The SOGI behaves like a band pass filter with resonance frequency equal to the grid frequency (*f=50Hz*), hence it is capable to extract the positive and negative components. The positive angle-phase component is used to synchronize properly the MG. However, the grid frequency can be varied; hence an adaptive frequency loop named FLL block (frequency locked loop) is added to adapt the resonance frequency of the SOGI in real time.

The SOGI algorithm consists of two filters; a band pass filter allowing the reconstitution of the filtered input signal *Vαβ'* and a low pass filter permitting the constitution of the in-quadrature component *qVαβ'*. The transfer function of the second order generalized integrator relating *Vαβ'* as well as *qVαβ'* to the *Vαβ* is given by

$$\frac{V_{\alpha\beta}'}{V_{\alpha\beta}} = \frac{k\,\omega' s}{s^2 + k\,\omega' s + \omega'^2} \tag{20}$$

$$\frac{qV_{\alpha\beta}'}{V_{\alpha\beta}} = \frac{k\,\omega'^2}{s^2 + k\,\omega' s + \omega'^2} \tag{21}$$

Where *ω'* is the *SOGI* resonance frequency and *k* is the damping factor. *Vαβ'* oscillates with the same frequency *ω'* of the input voltage while *qVαβ'* is the in-quadrature components of *Vαβ'*. These two parameters (*Vαβ'* and *qVαβ')* are used to calculate the positive and negative sequences for three phase systems, while they are themselves the positive and negative sequences in single phase system, and to calculate the proper

angle-phase.

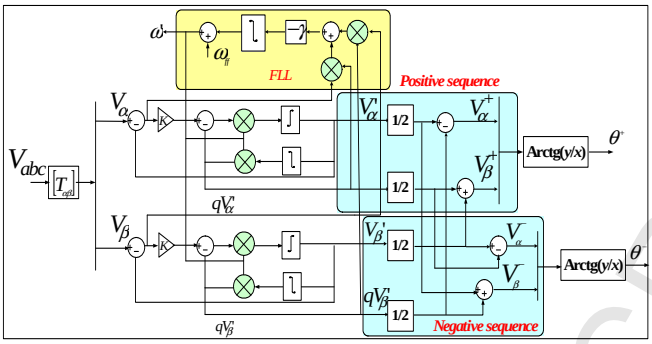

Fig. 8. Three-phase SOGI-FLL algorithm

3.4. Hybrid islanding method

The proposed islanding detection method is based on two parts, the first one aims to detect the variation of grid impedance parameters while the second one allows the determination of the grid impedance variation:

A. Passive part: The method based on temporal redundancies of grid current measurements is widely used and its efficiency in fault detection was proven [2]. Its principle consists on the detection of any abrupt variation between consecutive grid current measurements. Any abrupt current variation will be depicted as a residual with different amplitude levels. Indeed, in healthy state, with no grid impedance variation, the measured quantity current evolution has no discontinuity, hence the final residual noted Res_{igk}, calculated from three consecutive non-filtered residual noted r_k is lower than a small threshold ε. Once the grid impedance varies, in faulty state, the measured current quantity evolution will present a discontinuity shown as a residual spike at the instant of the grid fault. The residual expressions are given by Eq. (22) and Eq. (23).

$$\mathrm{Re}\, s_{igk} = r_k + r_{k-1} + r_{k-2} \tag{22}$$

$$r_k = \left| i_{gk} - 2i_{gk-1} + i_{gk-2} \right| \tag{23}$$

i_{gk}, i_{gk-1} and i_{gk-2} are the consecutive measured current at the acquisition sampling time T_a ; kT_a , $(k\text{-}1)T_a$ and $(k\text{-}2)T_a$. The threshold ε is defined as the maximum value that can reach Res_{igk} when current evolution has no discontinuity (Res_{igk},< ε) and since it is proportional to the square of the sampling, it will be always very small as expressed in Eq. (24) and Eq. (25).

$$\varepsilon = 3\omega^2 Ta^2 I_m \tag{24}$$

$$I_m = \frac{V_{PCCm} - V_{gm}}{\left| Z_g \right|} \tag{25}$$

Where V_{PCCm} is the maximum voltage at PCC, V_{gm} is the maximum grid voltage, and $\tau_s (\omega = 2\pi / \tau_s)$ is the system time constant, with $\tau_s <<< T_a$.

B. Active part: As proven in [3], the system resonance frequency depends on the grid impedance, especially on the inductive part of the grid impedance. The active part of the proposed hybrid islanding detection method allows the injection of the proper system resonance frequency needed to estimate the grid impedance parameters value once a grid fault occurs. In fact, the resonance is excited properly by a virtual damping resistance noted R_v that drives the system near the resonance once a residual spike is detected. Indeed, the principle of the method consists on taking a high proportional gain in the beginning, and then reducing the virtual resistance gradually until reaching the resonance. Then, in the next step the resonance frequency can be extracted by using the Fast Fourier Transformation (FFT). The resonance frequency of closest DGS responsible for islanding detection (indicated as part I in Fig.9), the estimated grid inductive part and the deduced grid resistive part are expressed as follows:

$$f_{res} = \frac{1}{2\pi}\sqrt{\frac{L_1 + L_2 + L_{line1} + L_g}{L_1 (L_2 + L_{line1} + L_g) C_f}} \tag{26}$$

$$\hat{L}_g = \frac{(L_1 + L_2 + L_{line1}) - (4\pi^2 L_1 (L_2 + L_{line1}) C_f \, {f_{res}}^2)}{(4\pi^2 L_1 C_f \, {f_{res}}^2 - 1)} \tag{27}$$

$$\hat{R}_g = \sqrt{\frac{9\omega^4 Ta^4}{\varepsilon^2}(V_{PCCm} - V_{gm})^2 - (\omega L_g)^2} \tag{28}$$

4. Simulation results

Simulations were carried out by using PSIM software. The proposed islanding detection method described for detection and estimation of grid impedance variation is tested on the system depicted in Fig.9. The parallel-inverters and different kinds of local loads are connected to a PCC. The linear resistive load is continuously connected but the linear resistive-inductive load (L_L) is connected at t_{ON}=0.8s and the non-linear one at t_{ON}=1.2s. The loads are sized to test their effect on islanding algorithm. The system parameters used in simulations are shown in Table 2, 3 and 4. In the second and third scenario, the voltage and frequency references are proposed by the system itself with E_{ref}=325V and ω_{ref}=314.159 rad/s.

Table 2. DGSs parameters

P_{DG1}	P_{DG2}	P_{DG3}	V_{DC}(V)	f_{PWM}	L_1	L_2	C_f	Z_g	Z_d
2kW	2kW	4kW	650	10kHz	2mH	2mH	25µ	0.4Ω, 0.9mH	2mH

Table 3. Loads parameters

Rp	Rl	Ll	Rnl	Lnl	Cnl
55Ω	128Ω	0.204H	80Ω	0.204H	2µF

Table 4. Control parameters

k_{pex}	k_{iex}	k_p	k_i	k_{pv}	k_{iv}	ω_c	ω_f	R_v	m	md	n	nd	T_a
24	7500	2	180	0.9	50	4	8	35	0.00027	0.000028	0.02	0.12	5µ

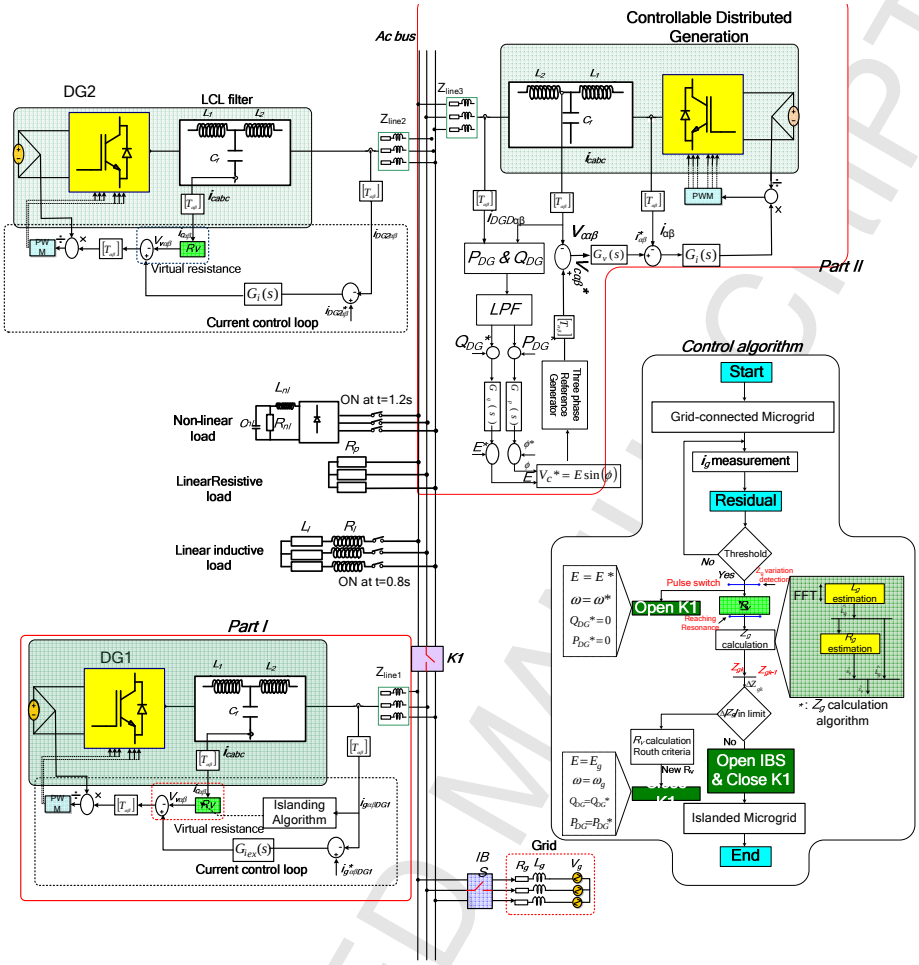

Fig.9. Proposed MG control structure

An abrupt grid fault is carried out by varying the grid impedance (from Z_g to Z_g+Z_d) at *t=1.24s*. The implemented passive part of the proposed islanding method based on residual calculation detects this variation successfully by presenting a residual spike. Then, the switch K_1 is opened to isolate the part of system composed of the closest DGS from the grid (DG1), the controllable DG and the non-controllable DG2 from the whole microgrid system. Finally, the active part of the proposed hybrid method is applied by exciting the resonance as shown in Fig. 10.

After the excitation during a specific period chosen here *1200* time of $T_{sampling}$, the algorithm will take the appropriate decision; reclosing the switch K_1 to reconnect the whole microgrid to the grid (scenario3) or going to scenario 4 and disconnect it from the utility grid to operate in islanding mode. As Z_d=*2mH*, which presents an impedance variation of 0.638Ω (ΔZ_g< 1 Ω), the switch K_1 is reclosed and scenario 3 is achieved. Noteworthy that before reclosing the switch K_1, the adaptive virtual resistance R_v can change its value to reconfigure the system with the new grid impedance parameters to maintain the system power quality.

Fig.11 shows the spectral analysis of the non-controllable DG1 current output. A spike at the frequency *f*=861Hz is presented. This frequency corresponds to the excited resonance frequency. Hence, the new grid impedance is estimated (f_{res}=861Hz➔ Estimated L_g=*2.7mH*)

Fig.12 presents the active and reactive powers of the non-controllable DG1and DG2 acting as a current sources and the controllable DG. The active powers of non-controllable DGSs are set to 2kW, *PD1=PD2=2kW*, while the controllable active power reference is chosen *4kW*. As shown in Fig. 12, in grid-connected controllable DGS, there is no-grid impedance variation and K_1 is closed. In this case, the controllable DGS proposes its powers references. In scenario 2, under resonance excitation, the loads require the needed power, hence the active P_{DG} and reactive Q_{DG} powers do not track their references and they just inject the rest of the required loads power none supplied by DG2.

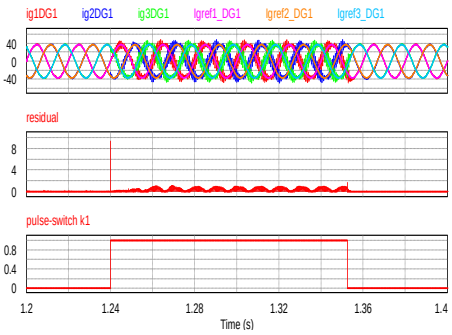

Fig. 10. Z_g variation detection and resonance excitation

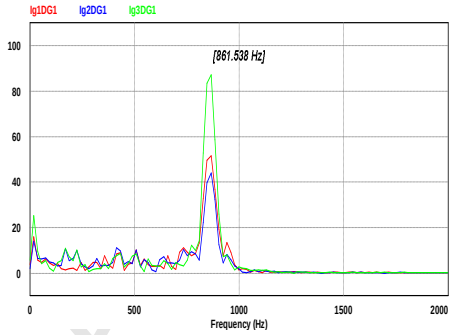

Fig.11. Resonance frequency (Z_d=*2mH*)

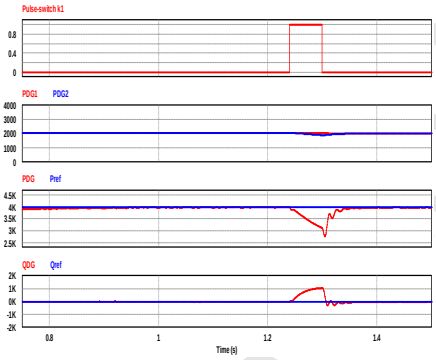

Fig. 12. DGSs output during the transition between scenarios

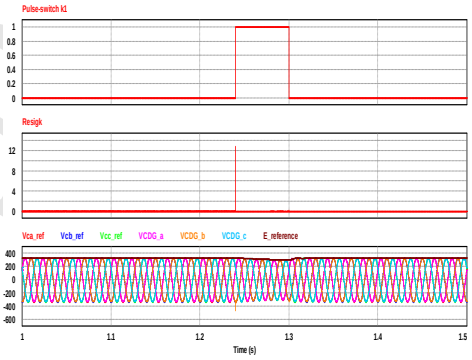

Fig. 13. Controllable DGS output voltage during resonance

The LCL-filter capacitor voltage in the controllable DGS noted by V_c is illustrated in Fig. 13, where the resonance effect does not appear. Its amplitude follows the voltage amplitude obtained at the output of the droop control algorithm, noted as *E-reference*. *E-reference* decreases during the resonance state due to the change of voltage amplitude reference as presented in Fig. 9, part '*Control algorithm*'.

It should be noted that the resonance excitation duration is chosen here, and in all next simulation results, equal to 800 times the $T_{sampling}$. This duration is lower than the time required by standards (*0.2s*) to detect islanding mode. It depends on the period of FFT window that necessities 2^N (2^N=126, 256, 512…) sampling times and can be less than the chosen duration. Indeed, the choice of this long period aims to show up the capability of the virtual resistance for resonance controlling by pushing the system near the resonance without diverges.

Fig. 14 shows the voltage at PCC supported by the controllable DGS under resonance excitation and by the utility grid over the resonance. The PCC voltage tracks its reference, noted E_{pcc}, reduced during the resonance state due to the disconnection of the controllable DG3 from the utility grid and to its relation to the reactive power demanded by the loads. Notice that the frequency presents a little variation in this state due to the relation *P*/*f* with the active power consumed by the loads.

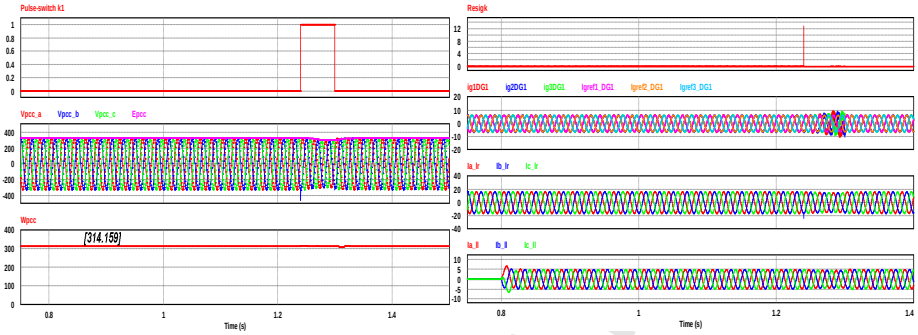

Fig.14. PCC voltage and frequency during resonance excitation

Fig. 15. Loads power quality during algorithm execution

As presented in Fig. 15, linear resistive and resistive-inductive loads are connected to the AC bus at different times to emphasize the effect of an abrupt load variation on the islanding detection method. The simulation results show that the proposed islanding detection method does not have any negative effect on the load current.

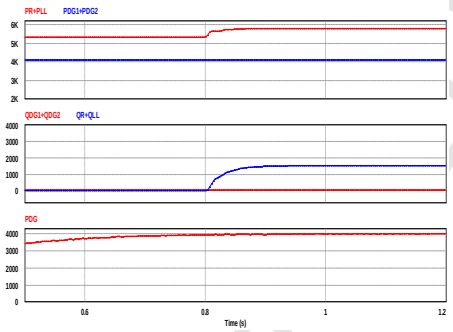

Fig. 16. Loads power under resonance excitation

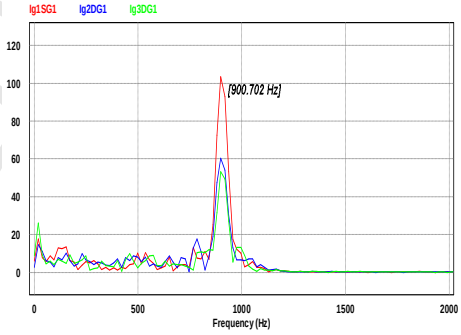

Fig. 17 Resonance frequency (Zd=1mH)

The relations presented in Eq. (1) and Eq. (2) are presented in Fig. 16, where the total loads power is higher than the powers supplied by both of the non-controllable DG1 and DG2. The active power P_{DG} of the controllable DGS is constant and equal to its reference (P_{DGref}=4kW).
Fig. 17 presents the spectral response of the grid side current in DG1 that depicts the presence of a spike at f=900Hz due to the resonance phenomenon appearance. By identification, a grid inductance of L_g=*1.75mH* is estimated.
Indeed, the proposed hybrid method can be used to improve the MG output quality after the islanding detection. In fact, the method allows the estimation of grid impedance that varies under grid fault or grid blackout; hence if the estimated grid impedance value exceeds the limit the IBS will open to disconnect the MG. In other way, if it is below the limits (ΔZ_g<*1Ω*), the DGS control strategy should adopt the grid parameters to maintain the output power quality and to avoid the interaction effect; hence system control reconfiguration is needed. In the proposed MG structure, the virtual resistance is used not only to damp the system (DG1 and DG2) and to drive the system near the resonance to extract the grid parameters but also for system reconfiguration reasons. The virtual resistance has the ability to maintain the system poles location and hence maintaining the system stability and reliability by returning the system poles, changed due to grid impedance variation, to their initial places.

5. Conclusion

In the next decades, power quality and service continuity will be the most important features on which the research interests relies. For this reason, islanding conditions detection is well investigated in the microgrid power quality improvement, to ensure the seamless transition between the operating modes grid-connected and the islanded mode, and also for protection reasons. In this way, a hybrid islanding detection method is presented in specific MG structure. This islanding method is based on resonance injection after grid parameters variation detection and it is able to detect the islanding under worst conditions. Indeed, the algorithm is implemented in the closest DGS of MG to the grid to avoid the interaction between the parallel-inverters under resonance state and it is capable to reconfigure the system control strategy by introducing the new grid parameters. During resonance excitation and throughout islanded mode, controllable DGS is used to support the frequency and voltage of MG while the parallel inverters act as current sources. The proposed detection algorithm is a proper and efficient solution for both intentional and unintentional islanding detection while the proposed MG structure is well flexible in terms of high MG power quality maintaining.

References

[1] A. H. K. Alaboudy, H. H. Zeineldin, Islanding detection for inverter-based dg coupled with frequency-dependent static loads, IEEE Trans. Power. Deliv. (2011) 1053 – 1063.
[2] H. Berriri, M.W. Naouar, I. Slama-Belkhodja, Sensor fault tolerant control for wind turbine systems with doubly fed induction generator, ELECTRIMACS 2011, 6-8th June 2011, Cergy-Pontoise, France, 2011.
[3] W. Ghzaiel, M. Jebali-Ben Ghorbal, I. Slama-Belkhodja, J. M. Guerrero, A novel grid impedance estimation technique based on adaptive virtual resistance control loop applied to distributed generation inverters, IEEE conference in Power Electronics and Application (2013) 1 – 10.
[4] J. M. Guerrero, J. Matas, L. G. de Vicuna, M. Castilla, J. Miret, De-centralized control of parallel operation of distributed generation inverters using resistive output impedance, IEEE Trans. Ind. Appl. (2007) 994–1004.
[5] J. M. Guerrero, J. C. Vasquez, J. Matas, M. Castilla, L. G. de Vicuna, Control strategy for flexible microgrid based on parallel line-interactive UPS systems, IEEE Trans. Ind. Electron. (2009) 726–736.
[6] J. B. Jeong, H. J. Kim, Active anti-islanding method for PV system using reactive power control, IET Electronics Letters (2006) 1004–1005.
[7] Y. A. -R. I. Mohamed, E. F. El-Saadany, Adaptive decentralized droop controller to preserve power sharing stability of paralleled inverters in distributed generation microgrids, IEEE Trans. Power. Electron. (2008) 2806–2816.
[8] J. Rocabert, Gustavo M. S. Azevedo, A. Luna, J. M. Guerrero, J. I. Candela, P. Rodrıguez, Intelligent connection agent for three-phase grid-connected microgrids, IEEE Trans. Power. Electron. (2011) 2993 – 3005.
[9] P. Rodríguez , A. Luna , I. Candela , R. Mujal , R.Teodorescu , F. Blaabjerg, Multiresonant frequency-locked loop for grid synchronization of power converters under distorted grid conditions, IEEE Trans. Ind. Electron. (2011) 127 - 138.

[10] P. Rodriguez, A. Luna, R. S. Munoz-Aguilar, I. Etxeberria-Otadui, R. Teodorescu, F. Blaabjerg , A stationary reference frame grid synchronization system for three-phase grid-connected power converters under adverse grid conditions, IEEE Trans. Power. Electron. (2012) 99 - 112.

[11] S. Seman, J. Niiranen, A. Arkkio, Ride-through analysis of doubly fed induction wind-power generator under unsymmetrical network disturbance, IEEE Trans. Power. Syst. (2006) 1782-1789.

[12] A.V. Timbus, P. Rodriguez, R. Teodorescu, M. Ciobotaru, Line impedance estimation using active and reactive power variations, IEEE Power Electronics Specialists Conference (2007) 1273 -1279.

[13] R. Teodorescu, F. Blaabjerg, M. Liserre, P.C. Loh, Proportional-resonant controllers and filters for grid-connected voltage-source converters, IET Electric Power Applications, (2006) 750 - 762.

[14] H. Vahedi, M. Karrari, Adaptive fuzzy sandia frequency-shift method for islanding protection of inverter-based distributed generation, IEEE Trans. Power. Deliv, (2013) 84 – 92.

[15] J.C. Vasquez, J.M. Guerrero, A. Luna, P. Rodriguez, R. Teodorescu, Adaptive droop control applied to voltage-source inverters operating in grid-connected and islanded modes, IEEE Trans. Ind. Electron. (2009) 4088 4096.

[16] J. C. Vasquez, J. M. Guerrero, J. Miret, M. Castilla, L. G. Vicuna, Hierarchical control of intelligent Microgrid, IEEE Ind. Electron. Mag. (2010) 23-29.

[17] J. C. Vasquez, J. M. Guerrero, M. Savaghebi, R. Teodorescu, Modeling, analysis, and design of stationary reference frame droop controlled parallel three-phase voltage source inverters, IEEE Trans. Ind. Electron. (2013) 1271 – 1280.

[18] X. Wang, J. M. Guerrero, Z Chen, Control of grid interactive AC Mmicrogrids, IEEE conference in Industrial Electronics (ISIE) (2010) 2211 - 2216

[19] Y. Zhu, D. Xu, N. He, J. Ma, J. Zhang, Y. Zhang,G. Shen, C. Hu, A Novel RPV (Reactive-Power-Variation) Antiislanding method based on adapted reactive power perturbation, IEEE Trans. Power. Electron. (2013) 4998 – 5012.